Clim. Past Discuss., 11, 243–278, 2015
www.clim-past-discuss.net/11/243/2015/
doi:10.5194/cpd-11-243-2015

Climate of the Past Discussions
Open Access

Onset of the Paleocene–Eocene Thermal Maximum in the southern Pacific Ocean (DSDP Site 277, Campbell Plateau)

C. J. Hollis[1], B. R. Hines[2], K. Littler[3,4], V. Villasante-Marcos[5], D. K. Kulhanek[6], C. P. Strong[1], J. C. Zachos[3], S. M. Eggins[7], L. Northcote[8], and A. Phillips[1]

[1]GNS Science, P.O. Box 30-368, Lower Hutt 5040, New Zealand
[2]School of Geography, Environment and Earth Sciences, Victoria University of Wellington, Wellington, New Zealand
[3]Earth and Planetary Sciences, University of California – Santa Cruz, CA 95060, USA
[4]Camborne School of Mines, University of Exeter, Penryn Campus, Cornwall, TR10 9FE, UK
[5]Observatorio Geofísico Central, Instituto Geográfico Nacional, 28014 Madrid, Spain
[6]International Ocean Discovery Program, Texas A&M University, College Station, TX 77845-9547, USA
[7]Research School of Earth Sciences, The Australian National University, Canberra 0200, ACT, Australia
[8]National Institute of Water and Atmosphere, P.O. Box 14901, Wellington, New Zealand

Received: 3 December 2014 – Accepted: 11 December 2014 – Published: 12 February 2015

Correspondence to: C. J. Hollis (c.hollis@gns.cri.nz)

Published by Copernicus Publications on behalf of the European Geosciences Union.

Abstract

Re-examination of a sediment core collected by the Deep Sea Drilling Project (DSDP Site 277) on the western margin of the Campbell Plateau, Southwest Pacific Ocean (paleolatitude of ~ 65° S), has identified an intact Paleocene–Eocene (P–E) boundary overlain by a 34 cm-thick record of the initial phase of the Paleocene–Eocene Thermal Maximum (PETM) within nannofossil chalk. The upper part of the PETM is truncated, either due to drilling disturbance or a sedimentary hiatus. An intact record of the onset of the PETM is indicated by a gradual decrease in δ^{13}C values over 20 cm, followed by a 14 cm interval in which δ^{13}C is 2 ‰ lighter than uppermost Paleocene values. After accounting for effects of diagenetic alteration, we use δ^{18}O and Mg/Ca values from foraminiferal tests to determine that intermediate and surface waters warmed by ~ 6° at the onset of the PETM prior to the full development of the negative δ^{13}C excursion. After this initial warming, sea temperatures were relatively stable through the PETM, but declined abruptly across the unconformity that truncates the event at this site. Mg/Ca analysis of foraminiferal tests indicate peak intermediate and surface water temperatures of ~ 19 and ~ 32 °C, respectively. These temperatures may be influenced by enhanced poleward ocean heat transport during the PETM and surface water values may also be biased towards warm season temperatures.

1 Introduction

Stable isotope analysis of foraminiferal tests from sediments cored at DSDP Site 277 (Shackleton and Kennett, 1975) provided the first paleotemperature record for the Paleogene of the Southern Ocean and laid the foundation for many subsequent studies of the regional paleoclimate and paleoceanography (e.g., Kennett, 1977, 1980; Kennett and Shackleton, 1976; Hornibrook, 1992; Nelson and Cook, 2001). Over the last decade, there has been renewed interest in the early Paleogene (66–35 Ma) climate history of the Southern Ocean, partly driven by a societal imperative to understand

CPD
11, 243–278, 2015

how the Antarctic ice sheet will respond to anthropogenic global warming (e.g., Joughin et al., 2014). The early Paleogene was the last time that Earth experienced greenhouse gas levels in excess of ~ 600 ppm CO_2 (Zachos et al., 2008; Beerling and Royer, 2011), and therefore provides insight into a climate state that civilization may experience in coming centuries. One event in particular has been touted as a geological analogue for greenhouse gas-driven global warming: the Paleocene–Eocene Thermal Maximum (PETM, ~ 56 Ma). This event was a short-lived (~ 220 kyr) perturbation to the climate and carbon cycle in which global temperatures rose by 4–5 °C within a few thousand years (Sluijs et al., 2007; McInerney and Wing, 2011; Dunkley-Jones et al., 2013; Schmidt, 2014), with warming of up to 8 °C in higher latitudes and some coastal settings (Thomas et al., 2002; Sluijs et al., 2006, 2011; Zachos et al., 2006; Hollis et al., 2012; Frieling et al., 2014). Multiple lines of evidence suggest that this warming may have been driven by a rapid injection of greenhouse gases, possibly sourced from submarine gas hydrates, as evidenced by coupled negative excursions in oxygen and carbon isotopes (Dickens et al., 1995, 1997). Several other potential sources of the light carbon have also been implicated to account for all or part of the carbon isotope ($\delta^{13}C$) excursion (Dickens, 2003, 2011; Kent et al., 2003; Svensen et al., 2004; Higgins and Schrag, 2006; De Conto et al., 2012).

The PETM has been identified in several sites in the Southwest Pacific, including onshore records in both siliciclastic and pelagic bathyal sections in eastern New Zealand (Kaiho et al., 1996; Crouch et al., 2001; Hancock et al., 2003; Hollis et al., 2005a, b, 2012; Nicolo et al., 2010), non-marine to marginal marine sediments in western New Zealand (Handley et al., 2011) and in shelfal sediments at Ocean Drilling Program (ODP) Site 1172, offshore eastern Tasmania (Sluijs et al., 2011). Here we report a new record of the PETM in pelagic bathyal sediments at DSDP Site 277, at a similar paleolatitude to Site 1172 (~ 65° S). These two sites represent the southernmost records of the PETM in the Pacific Ocean (Fig. 1).

Initial studies of Site 277 suggested that the Paleocene–Eocene (P–E) boundary occurred within a gap between cores 43 and 44 (Kennett et al., 1975). A subsequent

CPD
11, 243–278, 2015

biostratigraphic review of the site (Hollis et al., 1997) revealed that the boundary was lower in the drillhole, potentially within a relatively continuous interval preserved in core 45. Detailed re-sampling confirmed the location of the P–E boundary, based on the highest occurrence (HO) of benthic foraminifer *Stensionina beccariformis* at 457.3 mbsf (277-45-3, 80 cm). High resolution stable isotope analysis of bulk carbonate confirms that this horizon marks the base of a 34 cm-thick negative excursion in $\delta^{13}C$ that defines the PETM (Fig. 2).

DSDP Site 277 was drilled on the western margin of the Campbell Plateau in a water depth of 1214 m as part of DSDP Leg 29 (Kennett et al., 1975). Paleogene sedimentation occurred in fully oceanic conditions well above the lysocline (Kennett et al., 1975), with benthic foraminiferal assemblages indicating lower to middle bathyal water depths since the Paleocene (Hollis et al., 1997). In order to characterise sedimentary and paleoceanographic changes associated with the PETM at this site we have undertaken a multidisciplinary study that includes foraminiferal and calcareous nannofossil biostratigraphy, magnetic susceptibility, $CaCO_3$ content, elemental abundance using X-ray fluorescence (XRF), $\delta^{13}C$ and $\delta^{18}O$ analysis of bulk carbonate and foraminifera, and single test analysis of foraminifera for Mg/Ca ratios by Laser Ablation Inductively Coupled Plasma Mass Spectrometry (LA-ICPMS).

2 Material and methods

2.1 Material

We analysed samples over a 45 m interval spanning the upper Paleocene to lower Eocene at DSDP Site 277 (470–425 mbsf). Average sample spacing was 20 cm over much of the interval, with a higher resolution of 2–3 cm sampling across the PETM within core-section 45-3 (~ 457.30–456.95 mbsf). In addition, this core-section was scanned for elemental abundance. Although the PETM interval is preserved, the overall record is discontinuous, with significant gaps between cores from core 42–45 (Fig. 2).

CPD
11, 243–278, 2015

2.2 Methods

2.2.1 X-ray fluorescence (XRF) core scanning

XRF data were acquired using an Avaatech XRF scanner with a Canberra X-PIPS silicon drift detector, model SXD 15C-150-500 150 eV resolution X-ray detector, which is housed at the International Ocean Discovery Program (IODP) Gulf Coast Repository at Texas A&M University in College Station, Texas (Table S1 in the Supplement). This scanner is configured for analysis of split core section halves, with the X-ray tube and detector mounted on a moving track (Richter et al., 2006). Section 277-45-3 was removed from the core refrigerator and allowed to equilibrate to room temperature prior to analysis. We leveled all rock pieces within the section, as the detector requires a flush surface with no gaps between pieces, and then covered the section with 4 µm thick Ultralene plastic film (SPEX Centriprep, Inc.) to protect the detector. The section was scanned at 2 mm intervals using a voltage of 10 kV for elements Al, Si, P, S, Cl, Ar, K, Ca, Ti, Cr, Mn, Fe, Rh, and Ba. The scan was completed using a 1 mA tube current, no filter, and a detector live time of 30 s, with an X-ray detection area of 2 mm in the downcore direction and 15 mm across the core. During measurement, intervals were skipped where gaps of more than ~ 2 mm existed between pieces. Smaller gaps were noted so that suspect data across these gaps could be removed.

2.2.2 Rock magnetism

Bulk magnetic susceptibility of a subset of discrete samples was measured at the Paleomagnetism Laboratory of the Complutense University of Madrid, Spain (Table S2). A KLY-4 (Agico) susceptibility bridge was employed, with an applied magnetic field of 300 $A\,m^{-1}$. Due to the low ferromagnetic content of most of the samples, each sample was measured ten times and averaged. The error bars of the magnetic susceptibility data correspond to the SD of the mean (1σ) obtained during the averaging procedure.

CPD
11, 243–278, 2015

2.2.3 Micropaleontology

Calcareous nannofossil and foraminifera sample preparation and examination followed standard procedures. Samples for calcareous nannofossils were prepared using standard smear-slide techniques (Bown and Young, 1998). A small amount of sediment was mixed with a drop of water on a coverslip, distributed with a toothpick, and then dried on a hot plate. The coverslip was affixed to a glass microscope slide using Norland Optical Adhesive 61 and cured under an ultraviolet light. Slides were examined on a Leitz Ortholux II POL-BK microscope under cross-polarized and plane-transmitted lights. Counts of 400 specimens were conducted at 1000×, followed by a scan of at least 400 fields of view at 630× to look for rare taxa (Table S3).

Foraminiferal distribution was determined for 59 samples extending from the Paleocene to late early Eocene (Teurian to Mangaorapan local stages) (Table S4). Foraminiferal biostratigraphy is correlated with New Zealand stages (Cooper, 2004) and international biozones (Olsson et al., 1999; Pearson et al., 2006). New Zealand stage and biozone boundaries are calibrated to the 2012 geological timescale (Gradstein et al., 2012) using criteria described by Hollis et al. (2010) and Norris et al. (2014). Foraminiferal taxonomy is based on Hornibrook et al. (1989). Biostratigraphic results for calcareous nannofossils are correlated to the biostratigraphic zonation scheme of Martini (1970, 1971), calibrated to the 2012 geological timescale (Gradstein et al., 2012). Taxonomic concepts for species are those given in Perch-Nielsen (1985) and Bown (1998).

2.2.4 Stable isotopes and carbonate content

Analysis for stable isotopes and carbonate content was undertaken at three laboratories. Results are tabulated in Table S5. Bulk carbonate $\delta^{13}C$ and $\delta^{18}O$ measurements were undertaken at the National Isotope Centre, GNS Science, Lower Hutt. Samples were analysed on the GVI IsoPrime Carbonate Preparation System at a reaction temperature of 25 °C and run via dual inlet on the IsoPrime mass

CPD
11, 243–278, 2015

spectrometer. All results are reported with respect to VPDB, normalized to the GNS marble internal standard with reported values of 2.04 ‰ for δ^{13}C and −6.40 ‰ for δ^{18}O. The external precision (1σ) for these measurements is 0.05 ‰ for δ^{13}C and 0.12 ‰ for δ^{18}O.

Individual specimens from five foraminiferal genera were used for δ^{13}C and δ^{18}O and Mg/Ca analysis. Samples were selected based on light microscope assessment of preservation, which was subsequently confirmed by scanning electron microscope (SEM) examination. The genera used include two near-surface dwelling genera, *Morozovella* and *Acaranina*, the thermocline dweller *Subbotina* and two benthic genera, *Cibicides* and *Stensioina.*

Stable isotope analysis of foraminifera was carried out in the Stable Isotope Laboratory at the University of California, Santa Cruz. Between 1 and 6 (average of 3) specimens of *Cibicides*, 1 and 5 (average of 3) specimens of *Stensioina*, 3–17 (average of 10) specimens of *Acarinina*, 2–10 (average of 4) specimens of *Morozovella*, and 1–8 (average of 5) specimens of *Subbotina* were used in each analysis. Specimens were first sonicated in deionised water to remove clay and detrital calcite. Isotopic measurements were carried out on a Thermo-Finnigan MAT253 mass spectrometer interfaced with a Kiel Device. The analytical precision (1σ) is based on repeat analysis of an in-house standard (Carrara marble), calibrated to the international standards NBS18 and NBS19, and averages ±0.05 ‰ for δ^{13}C and ±0.08 ‰ for δ^{18}O. All values are reported relative to VPDB.

Paleotemperatures for both benthic and planktic taxa were calculated from δ^{18}O using the equation of Kim and O'Neil (1997):

$$T(^{\circ}\mathrm{C}) = 16.1 + -4.64(\delta^{18}\mathrm{O_M} - \delta^{18}\mathrm{O_{SW}}) + 0.09(\delta^{18}\mathrm{O_M} - \delta^{18}\mathrm{O_{SW}})^2 \quad (1)$$

Where $\delta^{18}\mathrm{O_M}$ = measured value and $\delta^{18}\mathrm{O_{SW}}$ = −1.46 ‰, which is the inferred value for sea water adjusted for paleolatitude (Zachos et al., 1994; correction of −0.23 ‰) and ice-free conditions (assuming ice-free ocean values of = −1 ‰).

CPD
11, 243–278, 2015

The carbonate content of dried powdered samples was determined at the National Institute of Water and Atmosphere (NIWA, Wellington) via gasometric quantitative analysis after acidification (Jones and Kaiteris, 1983), with a precision of ±2 %.

2.2.5 Elemental geochemistry and Mg/Ca analysis

Foraminifera were picked from the 150–300 µm fraction of washed sediment samples and individually washed in ultra-pure (> 18.2 mΩ) water and analytical grade methanol three times before being mounted on double-sided tape adhered to a glass slide. Wherever possible, the species *Morozovella crater*, *Acarinina primitiva* and *Cibicides eocaenus* were selected. Where these species were not available, *M. lensiformis*, *A. collactea* and *C. truncatus* were substituted. *Subbotina* was not subdivided beyond the genus level.

Mg/Ca analysis was carried out on samples composed of 4–19 specimens for each of the selected genera in each sample (Table S6). Each foraminifer was analysed at least three times using a pulsed Ar-F excimer laser (Lambda Physik LPFpro 205) with a 193 µm wavelength, 30 µm spot size, laser power of 3 J cm^{-2} and a repetition rate of 3 Hz, in conjunction with an ANU HelEx laser ablation cell, at the Research School of Earth Sciences of the Australian National University. An analysis of the NIST-SRM610 silicate standard was taken between every 9 and 12 foraminifer analyses to correct for elemental fractionation originating from laser ablation and mass-spectrometry effects.

The final three chambers of the final whorl in each specimen were analysed individually by ablating slowly at a rate of 0.2–0.3 µm s^{-1} to produce a separate trace element profile through the wall of each chamber. A Varian 820 ICPMS was used to measure abundances of the trace metal isotopes ^{24}Mg, ^{27}Al, ^{29}Si, ^{47}Ti,^{55}Mn, ^{66}Zn,^{88}Sr and ^{138}Ba relative to ^{43}Ca during ablation. Elemental ratios reported in this study are the average of the multiple chamber profiles measured in individual foraminifer specimens. Laser ablation sites were selected to avoid zones of detrital contamination, recrystallization or test ornamentation which might cause irregular trace element/Ca profiles.

CPD
11, 243–278, 2015

The extraction of a reliable paleotemperature record from variably preserved foraminifera is dependent on the preservation of primary foraminiferal calcite, and its inherent geochemical signature. In addition to using reflected light microscopy and SEM imaging to qualitatively screen tests for preservation, stringent screening criteria were applied to exclude zones within test wall profiles that show evidence of diagenetic alteration or silicate contamination as evident from anomalous Mg/Ca, Al/Ca, Mn/Ca, Ba/Ca and Sr/Ca ratios (Barker et al., 2003; Greaves et al., 2005; Creech et al., 2010). Individual trace element profiles typically show zones of substantially elevated Mg/Ca, Al/Ca and Mn/Ca ratios on the outside and inside surfaces of the foraminifera test wall, indicating siliciclastic sediment contamination, whereas Sr/Ca typically occurs at uniform levels throughout the test. Concentration may decrease or increase during alteration or secondary calcification (Eggins et al., 2003). Thus, samples with Sr/Ca values outside the range of 0.8–1.6 mmol mol^{-1} were considered to be affected by diagenesis (Fig. 3).

Al/Ca and Mg/Ca data show a positive linear correlation when plotted, reflecting the influence of alumino-silicate mineral contamination. This contamination has been screened out using the method of Creech (2010) after Barker et al. (2003). The Al/Mg composition of the contaminant phase was identified by plotting Mg/Ca against Al/Ca and finding the slope of the linear regression. Once this Mg/Al composition had been determined, the screening threshold was set by calculating the Al/Ca ratio at which paleotemperature estimates would be biased by more than 1 °C. This involved determining the corresponding Mg/Ca excess value by multiplying the observed mean Mg/Ca ratio for each species by the sensitivity of the paleotemperature calibration (i.e. an increase of 9 % in Mg/Ca per 1 °C after Anand et al., 2003). Once determined the Mg/Ca excess value for each species is multiplied by the Al/Mg contaminant phase to determine the Al/Ca ratio at which the screening threshold is set. This methodology circumvents the inclusion of artificially inflated paleotemperature estimates arising from silicate contamination (Fig. 3). The resulting reduction in average Mg/Ca ratios of the screened compared to the unscreened and data is shown in Fig. 3.

CPD
11, 243–278, 2015

The application of these screening limits to trace element data means that no Mg/Ca marine temperatures in this study should be overestimated by more than 1 °C (as a result of post-mortem diagenetic effects or sedimentary contamination).

Marine paleotemperatures are calculated using the exponential relationship between Mg/Ca and temperature (Eq. 2). Because the planktic foraminifera used in this study are extinct, sea surface temperatures (SSTs) were calculated using a general calibration based on the mean calcification temperatures of nine modern planktic species ($A = 0.09$, $B = 0.38$; Anand et al., 2003). Sea floor temperatures (SFTs) were calculated using the calibration of Lear et al. (2002) based on three benthic *Cibicidoides* species ($A = 0.109$, $B = 0.867$).

$$\mathrm{Mg/Ca_{test}} = \left(\frac{\mathrm{Mg/Ca_{sw}^{t=t}}}{\mathrm{Mg/Ca_{sw}^{t=1}}}\right) \cdot B \exp^{AT} \quad (2)$$

Marine temperature reconstructions based on early Eocene foraminiferal calcite have shown that a high ($> 3\,\mathrm{mol\,mol^{-1}}$) $\mathrm{Mg/Ca_{sw}}$ value is necessary to reconcile Mg/Ca-derived paleotemperatures with those derived from $\delta^{18}O$ (Lear et al., 2002; Sexton et al., 2006). Such high $\mathrm{Mg/Ca_{sw}}$ values are at odds with several proxy studies (e.g., Horita et al., 2004; Coggon et al., 2010) and models (e.g., Stanley and Hardie, 1998), but are in line with modelled values from Wilkinson and Algeo (1989), and multi-proxy paleotemperature reconstructions (Hollis et al., 2012). Lower values of Paleogene $\mathrm{Mg/Ca_{SW}}$ (e.g., Stanley and Hardie, 1998; Coggon et al., 2010) result in unrealistically high temperatures using Eq. (2). However, recent studies (Hasuik and Lohmann, 2010; Evans and Müller, 2012) have shown that a power law relationship, rather than an exponential relationship, may better describe the relationship between Mg-partitioning and temperature in foraminiferal calcite (Eq. 3).

$$\mathrm{Mg/Ca_{test}} = \left(\frac{B}{\mathrm{Mg/Ca_{sw}^{t=0^H}}}\right) \cdot \mathrm{Mg/Ca_{sw}^{t=t^H}} \exp^{AT} \quad (3)$$

CPD
11, 243–278, 2015

In applying this method, it is possible to derive realistic paleotemperatures using a lower Eocene Mg/Ca_{sw} value that is consistent with Mg/Ca_{sw} proxy evidence. Exponential and pre-exponential calibration constants from modern multispecies calibrations and paleotemperature values derived from oxygen isotopes can be utilised to estimate the function H for extinct foraminifera. Using published data from well-preserved Eocene foraminifera at Hampden Beach (Burgess et al., 2008; Hollis et al., 2012) and Tanzania (Pearson et al., 2007), for which paired Mg/Ca and $\delta^{18}O$ data is available, it is possible to derive the calibration correction constants (H) for the extinct species used in this study.

In calculating the value of H, we have used an early Eocene Mg/Ca_{sw} value of $1.6\,mol\,mol^{-1}$ (Stanley and Hardie, 1998; Evans and Müller, 2012) and a modern Mg/Ca_{sw} value of $5.17\,mol\,mol^{-1}$. The values of H determined for Paleogene foraminifera in this study are an approximation that do not take into account the likely fine scale variability in Mg/Ca_{sw} values through the early Paleogene. The Mg/Ca-temperature calibrations of Anand et al. (2003) and Lear et al. (2002) have been used, although it is likely that the pre-exponential constant of Paleogene planktic foraminifera differed from that of the modern taxa. The values of H calculated for Paleogene planktic foraminifera are lower ($H = 0.20$) than that for the modern taxon, *Globigerina sacculifer* ($H = 0.42$; Hasuik and Lohmann, 2010), possibly due to differences in Mg/Ca-temperature calibration. For benthic foraminifera, Cramer et al. (2011) suggest that the value of H would be similar between *Cibicides* sp. and *Oridorsalis umbonatus*. Mg/Ca-derived temperature values are calculated using Eq. (4).

$$T = \frac{\ln\left(\frac{\left[Mg/Ca_{test}\right] \times \left[Mg/Ca_{sw}^{t=0}\right]^{H}}{B \cdot \left[Mg/Ca_{sw}^{t=t}\right]^{H}}\right)}{A} \quad (4)$$

Temperature values derived from Mg/Ca ratios of surface mixed-layer dwelling taxa used in this study are normalised to *Morozovella crater* following Creech et al. (2010).

CPD
11, 243–278, 2015

Three types of error are applied to paleotemperatures derived from Mg/Ca ratios; the analytical error, sample error and a standard calibration error. The analytical error is accounted for in the data processing step, and typically produces very small uncertainties (±1–3 % 2se) associated with counting statistics during ablation and data acquisition. The sample error pertains to the 95 % confidence interval calculated for the mean temperature value obtained from multiple analyses within a single sample, and is calculated by:

$$\overline{X} \pm t \cdot \frac{\sigma}{\sqrt{n}} \quad (5)$$

Where $\overline{X}$ is the sample mean, t is the inverse of the Students' t distribution, σ represents the SD and n is the number of analyses. The calibration error is the residual error of ±1.6 °C on the regression of the multispecies calibrations established by Lear et al. (2002) and Anand et al. (2003). The cumulative error calculated from the sum of all three errors is applied to each temperature value, providing upper and lower uncertainties.

3 Results and discussion

3.1 Stratigraphy

The 45 m-thick studied interval (425–470 mbsf) consists of five cores, with significant gaps due to poor recovery in three of the cores, which extend from middle Paleocene to lower Eocene (Fig. 2). The sediments are greenish-white to greenish-grey nannofossil chalk, with higher clay content in the upper Paleocene (core 46; 463–470 mbsf) and lowermost Eocene (core-section 45-3; 456.96–457.3 mbsf)) and minor glauconite (cores 43-44) and chert nodules (cores 41–43) in the overlying Eocene. A record of "incipient chert" in core-section 45-3 (Kennett et al., 1973) may have been

CPD
11, 243–278, 2015

a misidentification of the darker-grey clay-rich sediments at the base of the PETM (Fig. 4).

Calcareous microfossils are moderately well preserved overall, although there is an interval directly below the Paleocene–Eocene boundary (457.3–457.58 mbsf) in which foraminifera are poorly preserved and sparse. Planktic foraminifera are used to correlate the 45 m-thick studied interval to New Zealand stages (Teurian to Mangaorapan) and to international foraminiferal zones P4a-b to E7 (Fig. 2). Nannofossil assemblages over the same interval have been correlated with nannofossil zones NP6 to NP12. Whereas previous studies indicated an undifferentiated upper Paleocene succession spanning Zone NP6–8 (Edwards and Perch-Nielsen, 1975; Hollis et al., 1997), we infer a ~2 Myr hiatus near the top of Core 46 (463.49–463.16 mbsf), representing all of zones NP7 and NP8. Immediately above the hiatus, *Discoaster multiradiatus* makes up ~2 % of the assemblage, suggesting that the first appearance datum (FAD) of this zonal marker (and thus the base of Zone NP9) is missing. This horizon marks the lowest occurrence (LO) of *Discoaster* at this site, including the LOs of *D. lenticularis* and *D. salisburgensis* in addition to *D. multiradiatus*.

The PETM is a 34 cm-thick interval within core 45 (457.3–456.96 mbsf) that is clearly delineated by a 40 % decrease in carbonate content and 2–3 ‰ negative excursions in bulk carbonate $\delta^{13}C$ and $\delta^{18}O$ values (Fig. 2). The location of the PETM is confirmed by biostratigraphy. The benthic foraminiferal extinction event (BFEE) is identified directly below the PETM at 457.3 mbsf based on the highest occurrences of the *Stensioina beccariformis*, *Gyroidinoides globosus* and *G. subangulatus*. For nannofossils, taxa typical of the PETM in other regions, such as the *Rhomboaster* lineage, *Discoaster araneus* and *D. anartios* (e.g., Bybell and Self-Trail, 1994; Kahn and Aubry, 2004), do not occur at Site 277. Instead, the nannofossil assemblage is characterized by deformed *Discoaster* specimens, many similar to *Discoaster nobilis* (e.g., Raffi and De Bernardi, 2008), as well as increased abundance of *Coccolithus* spp. and the presence of *Fasciculithus* spp. and *Bomolithus supremus*, which is restricted to the PETM interval at this site. Immediately above the PETM (456.92 mbsf), the

CPD
11, 243–278, 2015

abundances of *Fasciculithus* spp. and *Coccolithus* spp. decrease significantly, with a concomitant increase in *Zygrhablithus bijugatus*. As discussed below, the stable isotope record through the P–E transition indicates that the PETM is truncated, with only the onset of the CIE represented by these 34 cm of sediment.

The base of the PETM coincides with a distinct colour change to a darker greenish-grey chalk that grades back into greenish-white chalk over 15 cm (Fig. 4). This dark interval is also highly burrowed. Burrowing is also evident in other parts of the core but it is less obvious in more pale lithologies. XRF core scanning shows an increase in Fe content at the base of this interval, followed by a cyclical decrease to background levels at 456.95 m (Fig. 4a). Lower stratigraphic-resolution analysis of magnetic susceptibility in discrete samples reveals a similar trend: a peak near the base of the darker interval, followed by a quasi-cyclical decrease to background levels. An increase in clay content is inferred from the coupled increases in Fe and magnetic susceptibility and the decrease in carbonate content.

A 10 cm interval directly below the PETM also has a reduced carbonate concentration but there is no change in $\delta^{13}C$ and only a small positive shift in $\delta^{18}O$ of ~ 0.4 ‰ in both bulk and foraminiferal calcite (Fig. 2). As there is no accompanying increase in magnetic susceptibility or Fe content, the decrease in carbonate content seems to be due to an increase in silica, perhaps associated with the slight cooling indicated by the positive shift in $\delta^{18}O$. The cause of a peak in magnetic susceptibility and Fe content in the lower part of core 45 is unknown. There are no accompanying changes in isotopic signature and no obvious lithological changes.

An age-depth plot (Fig. 5) based on calcareous nannofossil and foraminiferal bioevents (Table S7) provides a preliminary guide to compacted sedimentation rates. This rate appears to have been relatively low in the Paleocene (0.4–0.45 cm kyr^{-1}), either side of the hiatus at $\sim$ 463.4 mbsf, but approximately four times higher in the early Eocene (1.68 cm kyr^{-1}). However, a rather patchy distribution of events and uncertainty over the presence and duration of hiatuses means that it is possible to construct an alternative age model in which rates were consistent across the Paleocene–Eocene

CPD
11, 243–278, 2015

transition (dashed line in Fig. 5). Although this implies that the sedimentation rate for the PETM interval could lie anywhere between the low Paleocene rate and the high Eocene rate, the lower rate is consistent with the duration of the onset known from other sites, i.e., 50–100 kyr (Zachos et al., 2008, 2010; Nicolo et al., 2010; McInerney and Wing, 2011). For a sedimentation rate of 0.4 cm kyr^{-1}, the 34 cm thick PETM interval represents ~ 85 kyr and the three peaks in Fe content represent a periodicity close to the precession band (19–22 kyr).

3.2 Stable isotopes and paleotemperatures

Bulk carbonate stable isotopes display a significant offset between δ^{18}O and δ^{13}C minima, with the δ^{18}O minimum occurring at the base of the PETM and the δ^{13}C minimum occurring at the top following a gradual decline (Figs. 2 and 4b). The negative δ^{13}C excursion of ~ 2 ‰ is slightly smaller than observed in most marine sections elsewhere (e.g., Nicolo et al., 2010; McInerney and Wing, 2011) and occurs gradually over the entire recovered PETM record. In contrast, the negative δ^{18}O excursion is abrupt at the base of the PETM and is far larger in magnitude than is known elsewhere (e.g., Zachos et al., 2008; McInerney and Wing, 2011). If this is a primary feature and due solely to a change in temperature, this 3 ‰ excursion would equate to ~ 12 °C of warming (Fig. 4d); however, it is most likely an artifact of diagenesis.

Examination of δ^{18}O values and Mg/Ca ratios within three genera of planktic foraminifera and one benthic genus provide insight into the nature of the diagenetic process. We suspect all shells have been altered to varying degrees. Based on visual and geochemical criteria, we were able to identify relatively well preserved tests. Isotopic analysis of those tests show that their bulk δ^{13}C values lie within the range of planktic foraminiferal δ^{13}C throughout the studied interval, with the exception of the base of the CIE (Fig. 6). In contrast, the bulk carbonate δ^{18}O values lie within the range of benthic foraminifer δ^{18}O in the Paleocene and in the Eocene interval above the PETM (Fig. 6). Moreover, planktic foraminiferal δ^{18}O is only slightly lighter than benthic and bulk δ^{18}O in the Paleocene (Figs. 2 and 6c). In contrast, bulk carbonate

CPD
11, 243–278, 2015

δ^{18}O values lie within the range of planktic foraminiferal δ^{18}O within the PETM (Fig. 6b) and, indeed, bulk carbonate δ^{18}O is lighter than planktic foraminiferal δ^{18}O in the basal PETM (Fig. 2).

We believe diagenetic effects explain these relationships. The bulk carbonate δ^{18}O has been shifted toward heavier values during early diagenesis (at seafloor temperature) over much of the section above and below the CIE (Schrag et al., 1995; Sexton et al., 1996), whereas within the PETM interval the bulk and foraminiferal carbonate has undergone little diagenetic alteration. We suspect the increase in clay content, as inferred from higher iron content (Fig. 4), slowed carbonate recrystallization, thus preserving the original δ^{18}O signal in the coccoliths and foraminifera within the PETM. High clay content reduces sediment porosity and retards carbonate recrystallization, almost completely in pure clays (e.g., Pearson et al., 2007; Burgess et al., 2008; Hollis et al., 2012). This explains the larger magnitude of the bulk carbonate δ^{18}O excursion across the P–E boundary, with the δ^{18}O values below the excursion having been altered toward heavier values (Figs. 2, 4d and e).

Similarly, the planktonic foraminiferal δ^{18}O values through the Paleocene–Eocene transition at DSDP Site 277 are compromised to varying degrees by seafloor diagenesis. Although the surface to deep temperature gradient may be expected to be reduced in high latitude regions such as the Campbell Plateau, the extremely small planktic-benthic offset in the Paleocene suggests alteration of planktic δ^{18}O toward benthic values. Temperature estimates derived from Mg/Ca ratios support our inference of a cool bias in planktic δ^{18}O due to seafloor diagenesis (Fog. 4d). There is limited opportunity for the Mg concentrations to be reset during diagenetic test recrystallization, in part because the bulk of Mg of the sediment/pore water system resides in the carbonate, whereas for oxygen isotopes, re-equilibration with ample supply of oxygen (in pore water) is possible. Consistent with the expected preservation biases, SST estimates of 26–27 °C derived from the Mg/Ca ratios of *Acarinina* are markedly warmer than the temperatures of 14–17 °C derived from planktic δ^{18}O.

CPD
11, 243–278, 2015

Benthic foraminifera tests are dense and thus less prone to recrystalization. Estimates for SFT from benthic foraminiferal $\delta^{18}O$ and Mg/Ca are remarkably consistent at 12–13 °C for the late Paleocene (Fig. 4d). Benthic $\delta^{18}O$ and Mg/Ca values indicate SFT warmed by ~ 5–6 °C across the P–E boundary, with SFTs of ~ 19 °C in the basal PETM. The planktic foraminiferal $\delta^{18}O$ values in the PETM yield SSTs of 26 °C, whereas Mg/Ca ratios within the PETM yield much warmer SST estimates of 28–32 °C (Fig. 4d). The peak SSTs of ~ 32° within the PETM are consistent with TEX_{86}-based SSTs from the PETM at ODP Site 1172, East Tasman Plateau (Sluijs et al., 2011), and in the mid-Waipara section, eastern South Island, New Zealand (Hollis et al., 2012). At these locations, the two calibrations for TEX_{86} introduced by Kim et al. (2010) yield peak SSTs for the PETM of 32–34 °C (TEX_{86}^{H}) or 26–28 °C (TEX_{86}^{L}). Although the TEX_{86}^{L} calibration was considered more suitable for this region based on comparisons with other SST proxies (Hollis et al., 2012), a new Bayesian approach to TEX_{86} calibrations (Tierney and Tingley, 2014) yields temperatures for the PETM that are very similar to the TEX_{86}^{H} calibration. These PETM SSTs are also consistent with the SST estimates of 26 °C that were derived from TEX_{86} and $U_{37}^{K'}$ for the late Eocene at Site 277 (Liu et al., 2009), given that deep sea temperatures cooled by ~ 8 °C through the Eocene (Zachos et al., 2008).

There is considerable debate about the veracity of such high temperature estimates in high latitude regions, with concerns raised about calibrations, seasonal bias and physiological processes (e.g. Hollis et al., 2012; Taylor et al., 2013; Inglis et al., 2015). However, the consistency between SSTs derived from Mg/Ca and TEX_{86} (Burgess et al., 2008; Hollis et al., 2012) suggests that the high temperatures are due to factors that the proxies may have in common, such as a warm-season bias, rather than problems with respective calibrations or physiological factors.

CPD
11, 243–278, 2015

3.3 Pattern of PETM initiation

Complications relating to diagenetic overprinting have been discussed and partly resolved in the previous section. To circumvent additional uncertainties surrounding absolute temperature estimates based on $\delta^{18}O$ values and Mg/Ca ratios (Cramer et al., 2011; Evans and Müller, 2012; Dunkley-Jones et al., 2013), it is helpful to consider temperature trends relative to mean values for the Paleocene (Fig. 4e). For both proxies, SFTs increase by 5–6 °C at the onset of the PETM, remain relatively stable through the PETM and decline abruptly across the unconformity that truncates the top of the event. Because the relative temperature trends shown by planktic $\delta^{18}O$ are inferred to be compromised by diagenesis, Mg/Ca ratios provide a more reliable guide to changes in local SST. In the basal part of the PETM, there are few planktic records that fall below the screening limit for Al/Ca (Fig. 3). Those specimens of *Acarinina* that are judged to be reliable indicate initial warming of SSTs by ~ 6 °C. For the upper part of the PETM, still likely representing the onset phase, Mg/Ca ratios for both *Acarinina* and *Morozovella* consistently indicate SSTs that are ~ 2 °C above average Paleocene values for *Acarinina* (Fig. 4d). Although this increase is within the error range for these measurements, the consistency between samples gives us reasonable confidence in the overall increase in temperature. This increase in SST is similar to other PETM records. At ODP Site 1172, the TEX_{86} record indicates that SST increased by 6 °C across the P/E boundary and SST during the PETM was 3–4 °C warmer than average Paleocene values (Fig. 7). Elsewhere, temperature anomalies within the PETM range from +4–5 °C in low latitudes (Zachos et al., 2003; Aze et al., 2014) to +8 °C in high latitudes (Thomas et al., 2002; Frieling et al., 2014) and some low latitude coastal sites (Zachos et al., 2006).

More detailed comparison of the PETM record at DSDP Site 277 with nearby records at Mead Stream (Hollis et al., 2005a; Nicolo et al., 2010) and ODP Site 1172 (Sluijs et al., 2011) reveals several significant features (Fig. 7). Firstly, there seems little doubt that only the onset of the PETM is preserved at Site 277. The pattern of

CPD
11, 243–278, 2015

decreasing $\delta^{13}C$ is very similar to the expanded onset at Mead Stream. However, the pattern of warming at Site 277 is quite different from the other sites. At Site 277, the most pronounced increase in temperatures occurs at the base of the PETM and is associated with a weak negative $\delta^{13}C$ excursion. Higher in the PETM, temperatures remain stable or decrease slightly as $\delta^{13}C$ decreases. At Site 1172, the TEX_{86} record indicates pronounced warming at the base of the PETM but SST continues to increase and peaks just above the $\delta^{13}C$ minimum. No direct measurements of temperature have been obtained from the indurated lithologies at Mead Stream. However, changes in radiolarian assemblages identify a definite peak in low-latitude species, also directly above the $\delta^{13}C$ minimum (red star in Fig. 7) (Hollis, 2006).

The implication of these differences between SW Pacific sites is that the primary warming pulse occurred in both intermediate and surface waters at the initiation of the PETM on the Campbell Plateau, whereas this initial event was only the precursor to progressive warming in the continental margin settings to the west and north (Fig. 1). It is important to note that we cannot be sure that there was not a second warming pulse above the onset of the PETM on the Campbell Plateau because the main phase of the PETM does not appear to be preserved at Site 277. However, it is equally important to note that the absolute SST values at Site 277 are similar to the peak SSTs at Site 1172, i.e. 30–32 °C. Therefore, we need to explain how the Campbell Plateau warmed at the start of the PETM and stayed warm through the onset, while the East Tasman Plateau warmed to a lesser extent initially but then continued to warm into the main phase of the PETM, with both sites experiencing at least seasonal SST maxima in excess of 30 °C. We speculate that the gradual warming that followed Southern Ocean cooling at 59 Ma (Hollis et al., 2014) exceeded a threshold at the start of the PETM that caused the southward expansion of the subtropical-tropical gyre over the Campbell Plateau. This gyre was sustained through the PETM onset but resulted in no additional warming at this location. The influence of the gyre may have also reached the East Tasman Plateau but an additional factor continued to warm the region into the main phase of

CPD
11, 243–278, 2015

the PETM. This factor may have been a proto-Eastern Australian Current, intensifying its southwestern reach during times of extreme warming (e.g. Cortese et al., 2013).

4 Conclusions

The onset of the PETM is recorded in a 34 cm thick interval within core 45 at DSDP Site 277. A significant and rapid warming of surface and deep waters at the onset of the PETM at Site 277 parallels a pronounced decline in carbonate concentration and a modest initial negative $\delta^{13}C$ excursion of ~ 1 ‰. The full extent of the 2 ‰ negative $\delta^{13}C$ excursion occurred gradually over an interval in which temperatures remained stable or declined slightly. Therefore, it would seem that an initial carbon perturbation had a pronounced effect on southern Pacific Ocean circulation, causing poleward expansion of warm surface and intermediate waters. In contrast, the full expression of the event had no additional effect, perhaps because a threshold was exceeded at the initial event.

The Supplement related to this article is available online at doi:10.5194/cpd-11-243-2015-supplement.

References

Anand, P., Elderfield, H., and Conte, M. H.: Calibration of Mg/Ca thermometry in planktonic foraminifera from a sediment trap time series, Paleoceanography, 18, 1050, doi:10.1029/2002PA000846, 2003.

Aze, T., Pearson, P. N., Dickson, A. J., Badger, M. P. S., Bown, P. R., Pancost, R. D., Gibbs, S. J., Huber, B. T., Leng, M. J., Coe, A. L., Cohen, A. S., and Foster, G. L.: Extreme warming of tropical waters during the Paleocene–Eocene Thermal Maximum, Geology, 42, 739–742, 2014.

CPD
11, 243–278, 2015

Barker, S., Greaves, M., and Elderfield, H.: A study of cleaning procedures used for foraminiferal Mg/Ca paleothermometry, Geochem. Geophy. Geosy., 4, 8407, doi:10.1029/2003gc000559, 2003.

Beerling, D. J. and Royer, D. L.: Convergent Cenozoic CO_2 history, Nat. Geosci., 4, 418–420, 2011.

Bown, P. R. (Ed.): Calcareous Nannofossil Biostratigraphy, Kluwer Academie, London, 315 p., 1998.

Bown, P. R. and Young, J. R.: Techniques, in: Calcareous Nannofossil Biostratigraphy, edited by: Bown, P. R., Kluwer Academie, London, 16–28, 1998.

Burgess, C. E., Pearson, P. N., Lear, C. H., Morgans, H. E. G., Handley, L., Pancost, R. D., and Schouten, S.: Middle Eocene climate cyclicity in the southern Pacific: implications for global ice volume, Geology, 36, 651–654, 2008.

Bybell, L. M. and Self-Trail, J. M.: Evolutionary, biostratigraphic, and taxonomic study of calcareous nannofossils from a continuous Paleocene–Eocene boundary section in New Jersey, US Geological Survey, Denver, Colorado, Professional Paper 1554, 114 p., 1994.

Coggon, R. M., Teagle, D. A. H., Smith-Duque, C. E., Alt, J. C., Cooper, M. J.: Reconstructing past seawater Mg/Ca and Sr/Ca from mid-ocean ridge flank calcium carbonate veins, Science, 327, 1114–1117, 2010.

Cooper, R. A.: The New Zealand Geological Timescale, Institute of Geological and Nuclear Sciences Monograph 22, Institute of Geological and Nuclear Sciences, Lower Hutt, 284 pp., 2004.

Cortese, G., Dunbar, G. B., Carter, L., Scott, G., Bostock, H., Bowen, M., Crundwell, M., Hayward, B. W., Howard, W., Martinez, J. I., Moy, A., Neil, H., Sabaa, A., and Sturm, A.: Southwest Pacific Ocean response to a warmer world: insights from Marine Isotope Stage 5e, Paleoceanography, 28, 1–14, doi:10.1002/palo.20052, 2013.

Cramer, B. S., Miller, K. G., Barrett, P. J., and Wright, J. D.: Late Cretaceous-Neogene trends in deep ocean temperature and continental ice volume: reconciling records of benthic foraminiferal geochemistry (δ^{18}O and Mg/Ca) with sea level history, J. Geophys. Res.-Oceans, 116, C12023, doi:10.1029/2011jc007255, 2011.

Creech, J. B., Baker, J. A., Hollis, C. J., Morgans, H. E. G., and Smith, E. G. C.: Eocene sea temperatures for the mid-latitude southwest Pacific from Mg/Ca ratios in planktonic and benthic foraminifera, Earth Planet. Sc. Lett., 299, 483–495, doi:10.1016/j.epsl.2010.09.039, 2010.

CPD
11, 243–278, 2015

Crouch, E. M., Heilmann-Clausen, C., Brinkhuis, H., Morgans, H. E. G., Egger, H., and Schmitz, B.: Global dinoflagellate event associated with the late Paleocene thermal maximum, Geology, 29, 315–318, 2001.

Crouch, E. M., Dickens, G. R., Brinkhuis, H., Aubry, M. P., Hollis, C. J., Rogers, K. M., and Visscher, H.: The *Apectodinium* acme and terrestrial discharge during the Paleocene–Eocene Thermal Maximum: new palynological, geochemical and calcareous nannoplankton observations at Tawanui, New Zealand, Palaeogeogr. Palaeocl., 194, 387–403, 2003.

Dickens, G. R.: Rethinking the global carbon cycle with a large, dynamic and microbially mediated gas hydrate capacitor, Earth Planet. Sc. Lett., 213, 169–183, 2003.

Dickens, G. R.: Down the Rabbit Hole: toward appropriate discussion of methane release from gas hydrate systems during the Paleocene–Eocene thermal maximum and other past hyperthermal events, Clim. Past, 7, 831–846, doi:10.5194/cp-7-831-2011, 2011.

Dickens, G. R., O'Neil, J. R., Rea, D. K., and Owen, R. M.: Dissociation of oceanic methane hydrate as a cause of the carbon isotope excursion at the end of the Paleocene, Paleoceanography, 10, 965–972, 1995.

Dickens, G. R., Castillo, M. M., and Walker, J. C. G.: A blast of gas in the latest Paleocene: simulating first-order effects of massive dissociation of oceanic methane hydrate, Geology, 25, 259–262, 1997.

Dunkley Jones, T., Lunt, D. J., Schmidt, D. N., Ridgwell, A., Sluijs, A., Valdes, P. J., and Maslin, M.: Climate model and proxy data constraints on ocean warming across the Paleocene–Eocene Thermal Maximum, Earth Sci. Rev., 125, 123–145, doi:10.1016/j.earscirev.2013.07.004, 2013.

Eggins, S., De Deckker, P., and Marshall, J.: Mg/Ca variation in planktonic foraminifera tests: implications for reconstructing palaeo-seawater temperature and habitat migration, Earth Planet. Sc. Lett., 212, 291–306, doi:10.1016/S0012-821X(03)00283-8, 2003.

Evans, D. and Müller, W.: Deep time foraminifera Mg/Ca paleothermometry: nonlinear correction for secular change in seawater Mg/Ca, Paleoceanography, 27, PA4205, doi:10.1029/2012PA002315, 2012.

Frieling, J., Iakovleva, A. I., Reichart, G.-J., Aleksandrova, G. N., Gnibidenko, Z. N., Schouten, S., and Sluijs, A.: Paleocene–Eocene warming and biotic response in the epicontinental West Siberian Sea, Geology, 42, 767–770, 2014.

Gradstein, F. M., Ogg, J. G., Schmitz, M., and Ogg, G.: The Geologic Time Scale 2012, Elsevier Science BV, Oxford, UK, 2012.

Greaves, M., Barker, S., Daunt, C., and Elderfield, H.: Accuracy, standardization, and interlaboratory calibration standards for foraminiferal Mg/Ca thermometry, Geochem. Geophy. Geosy., 6, Q02D13, doi:10.1029/2004GC000790, 2005.

Hancock, H. J. L., Dickens, G. R., Strong, C. P., Hollis, C. J., and Field, B. D.: Foraminiferal and carbon isotope stratigraphy through the Paleocene–Eocene transition at Dee Stream, Marlborough, New Zealand, New Zeal. J. Geol. Geop., 46, 1–19, 2003.

Handley, L., Crouch, E. M., and Pancost, R. D.: A New Zealand record of sea level rise and environmental change during the Paleocene–Eocene Thermal Maximum, Palaeogeogr. Palaeocl., 305, 185–200, 2011.

Hasiuk, F. J. and Lohmann, K. C.: Application of calcite Mg partitioning functions to the reconstruction of paleocean Mg/Ca, Geochim. Cosmochim. Ac., 74, 6751–6763, 2010.

Higgins, J. A. and Schrag, D. P.: Beyond methane: towards a theory for the Paleocene–Eocene Thermal Maximum, Earth Planet. Sc. Lett., 245, 523–537, 2006.

Hollis, C. J.: Radiolarian faunal change across the Paleocene–Eocene boundary at Mead Stream, New Zealand, Eclogae Geol. Helv., 99, S79–S99, 2006.

Hollis, C. J., Waghorn, D. B., Strong, C. P., and Crouch, E. M.: Integrated Paleogene biostratigraphy of DSDP site 277 (Leg 29): foraminifera, calcareous nannofossils, Radiolaria, and palynomorphs, Institute of Geological and Nuclear Sciences, Lower Hutt, Science Report 97/7, 1–73, 1997.

Hollis, C. J., Dickens, G. R., Field, B. D., Jones, C. J., and Strong, C. P.: The Paleocene–Eocene transition at Mead Stream, New Zealand: a southern Pacific record of early Cenozoic global change, Palaeogeogr. Palaeocl., 215, 313–343, 2005a.

Hollis, C. J., Field, B. D., Jones, C. M., Strong, C. P., Wilson, G. J., and Dickens, G. R.: Biostratigraphy and carbon isotope stratigraphy of uppermost Cretaceous-lower Cenozoic in middle Clarence valley, New Zealand, J. Roy. Soc. New Zeal., 35, 345–383, 2005b.

Hollis, C. J., Beu, A. G., Crampton, J. S., Crundwell, M. P., Morgans, H. E. G., Raine, J. I., Jones, C. M., and Boyes, A. F.: Calibration of the New Zealand Cretaceous-Cenozoic timescale to GTS2004, GNS Science, Lower Hutt, GNS Science Report 2010/43, 20 pp., 2010.

Hollis, C. J., Taylor, K. W. T., Handley, L., Pancost, R. D., Huber, M., Creech, J., Hines, B., Crouch, E. M., Morgans, H. E. G., Crampton, J. S., Gibbs, S., Pearson, P., and Zachos, J. C.: Early Paleogene temperature history of the Southwest Pacific Ocean: reconciling proxies and models, Earth Planet. Sc. Lett., 349–350, 53–66, 2012.

CPD
11, 243–278, 2015

Hollis, C. J., Tayler, M. J. S., Andrew, B., Taylor, K. W., Lurcock, P., Bijl, P. K., Kulhanek, D. K., Crouch, E. M., Nelson, C. S., Pancost, R. D., Huber, M., Wilson, G. S., Ventura, G. T., Crampton, J. S., Schiøler, P., and Phillips, A.: Organic-rich sedimentation in the South Pacific Ocean associated with Late Paleocene climatic cooling, Earth Sci. Rev., 134, 81–97, 2014.

Horita, J., Zimmermann, H., and Holland, H. D.: Chemical evolution of seawater during the Phanerozoic: implications from the record of marine evaporites, Geochim. Cosmochim. Ac., 66, 3733–3756, 2002.

Hornibrook, N. de B.: New Zealand Cenozoic marine paleoclimates: a review based on the distribution of some shallow water and terrestrial biota, in: Pacific Neogene: Environment, Evolution and Events, edited by: Tsuchi, R. and Ingle, J. C., University of Tokyo Press, Tokyo, 83–106, 1992.

Hornibrook, N. de B., Brazier, R. C., and Strong, C. P.: Manual of New Zealand Permian to Pleistocene foraminiferal biostratigraphy, Paleontological bulletin/New Zealand Geological Survey, 56, 1–175, 1989.

Inglis, G. N., Farnsworth, A., Lunt, D., Foster, G. L., Hollis, C. J., Pagani, M., Jardine, P. E., Pearson, P. N., Markwick, P., Raynman, L., Galsworthy, A. M. J., and Pancost, R. D.: Descent towards the Icehouse: Eocene sea surface cooling inferred from GDGT distributions, Paleoceanography, in review, 2015.

Jones, G. A. and Kaiteris, P.: A vacuum-gasometric technique for rapid and precise analysis of calcium carbonate in sediment and soils, J. Sediment. Petrol., 53, 655–660, 1983.

Joughin, I., Smith, B. E., and Medley, B.: Marine ice sheet collapse potentially under way for the Thwaites Glacier Basin, West Antarctica, Science, 344, 735–738, 2014.

Kahn, A. and Aubry, M.-P.: Provincialism associated with the Paleocene/Eocene thermal maximum: temporal constraint, Mar. Micropaleontol., 52, 117–131, 2004.

Kaiho, K., Arinobu, T., Ishiwatari, R., Morgans, H. E. G., Okada, H., Takeda, N., Tazaki, K., Zhou, G., Kajiwara, Y., Matsumoto, R., Hirai, A., Niitsuma, N., and Wada, H.: Latest Paleocene benthic foraminiferal extinction and environmental changes at Tawanui, New Zealand, Paleoceanography, 11, 447–465, 1996.

Kennett, J. P.: Initial reports of the Deep Sea Drilling Project, volume 29, US Govt. Printing Office, Washington, 1975.

Kennett, J. P.: Cenozoic evolution of Antarctic glaciation, the Circum-Antarctic Ocean, and their impact on global paleoceanography, J. Geophys. Res., 82, 3843–3860, 1977.

CPD
11, 243–278, 2015

Kennett, J. P.: Paleoceanographic and biogeographic evolution of the Southern Ocean during the Cenozoic, and Cenozoic microfossil datums, Palaeogeogr. Palaeocl., 31, 123–152, 1980.
Kent, D. V., Cramer, B. S., Lanci, L., Wang, D., Wright, J. D., and Van der Voo, R.: A case for a comet impact trigger for the Paleocene/Eocene thermal maximum and carbon isotope excursion, Earth Planet. Sc. Lett., 211, 13–26, 2003.
Kim, S.-T. and O'Neil, J. R.: Equilibrium and nonequilibrium oxygen isotope effects in synthetic carbonates, Geochim. Cosmochim. Ac., 61, 3461–3475, 1997.
Kim, J.-H., van der Meer, J., Schouten, S., Helmke, P., Willmott, V., Sangiorgi, F., Koç, N., Hopmans, E. C., and Damsté, J. S. S.: New indices and calibrations derived from the distribution of crenarchaeal isoprenoid tetraether lipids: implications for past sea surface temperature reconstructions, Geochim. Cosmochim. Ac., 74, 4639–4654, 2010.
Lear, C. H., Rosenthal, Y., and Slowey, N.: Benthic foraminiferal Mg/Ca-paleothermometry: a revised core-top calibration, Geochim. Cosmochim. Ac., 66, 3375–3387, 2002.
Liu, Z., Pagani, M., Zinniker, D., DeConto, R., Huber, M., Brinkhuis, H., Shah, S. R., Leckie, R. M., and Pearson, A.: Global cooling during the Eocene–Oligocene climate transition, Science, 323, 1187–1190, 2009.
Martini, E.: Standard Paleogene calcareous nannoplankton zonation, Nature, 226, 560–561, 1970.
Martini, E.: Standard Tertiary and Quaternary calcareous nannoplankton zonation, in: Proceedings of the Planktonic Conference II, Roma, 1970, edited by: Farinacci, A., Edizioni Tecnoscienze, Rome, 739–785, 1971.
McInerney, F. A. and Wing, S. L.: The Paleocene–Eocene Thermal Maximum: a perturbation of carbon cycle, climate, and biosphere with implications for the future, Annu. Rev. Earth Pl. Sc., 39, 489–516, 2011.
Nelson, C. S. and Cooke, P. J.: History of oceanic front development in the New Zealand sector of the Southern Ocean during the Cenozoic: a synthesis, New Zeal. J. Geol. Geop., 44, 535–553, 2001.
Nicolo, M. J., Dickens, G. R., Hollis, C. J., and Zachos, J. C.: Multiple early Eocene hyperthermals: their sedimentary expression on the New Zealand continental margin and in the deep sea, Geology, 35, 699–702, doi:10.1130/g23648a.1, 2007.
Nicolo, M. J., Dickens, G. R., and Hollis, C. J.: South Pacific intermediate water oxygen depletion at the onset of the Paleocene–Eocene thermal maximum as depicted in New Zealand margin sections, Paleoceanography, 25, PA4210, doi:10.1029/2009PA001904, 2010.

CPD
11, 243–278, 2015

Norris, R. D., Wilson, P. A., Blum, P., and Expedition 342 Scientists: Proceedings of the IODP 342, Washington, DC, doi:10.2204/iodp.proc.342.2014, 2014.
Olsson, R. K., Hemleben, C., Berggren, W. A., and Huber, B. T.: Atlas of Paleocene planktonic foraminifera, Sm. C. Paleob., 85, 1–252, 1999.
Pearson, P. N., Olsson, R. K., Huber, B. T., Hemleben, C., and Berggren, W. A.: Atlas of Eocene Planktonic Foraminifera, Cushman Foundation, Washington, DC, Special Publication no. 41, 514 pp., 2006.
Pearson, P. N., van Dongen, B. E., Nicholas, C. J., Pancost, R. D., Schouten, S., Singano, J. M., and Wade, B. S.: Stable warm tropical climate through the Eocene Epoch, Geology, 35, 211–214, 2007.
Perch-Nielsen, K.: Cenozoic calcareous nannofossils, in: Plankton Stratigraphy, edited by: Bolli, H. M., Saunders, J. B., and Perch-Nielsen, K., Cambridge University Press, Cambridge, 427–554, 1985.
Raffi, I. and De Bernardi, B.: Response of calcareous nannofossils to the Paleocene–Eocene Thermal Maximum: observations on composition, preservation and calcification in sediments from ODP Site 1263 (Walvis Ridge – SW Atlantic), Mar. Micropaleontol., 69, 119–138, 2008.
Rampino, M. R.: Peraluminous igneous rocks as an indicator of thermogenic methane release from the North Atlantic Volcanic Province at the time of the Paleocene–Eocene Thermal Maximum (PETM), B. Volcanol., 75, 1–5, 2013.
Richter, T. O., van der Gaast, S., Kaster, B., Vaars, A., Gieles, R., de Stigter, H. C., De Haas, H., and van Weering, T. C. E.: The Avaatech XRF core scanner: technical description and applications to NE Atlantic sediments, Geol. Soc. Spec. Publ., 267, 39–50, doi:10.1144/GSL.SP.2006.267.01.03, 2006.
Schmidt, G. A., Annan, J. D., Bartlein, P. J., Cook, B. I., Guilyardi, E., Hargreaves, J. C., Harrison, S. P., Kageyama, M., LeGrande, A. N., Konecky, B., Lovejoy, S., Mann, M. E., Masson-Delmotte, V., Risi, C., Thompson, D., Timmermann, A., Tremblay, L.-B., and Yiou, P.: Using palaeo-climate comparisons to constrain future projections in CMIP5, Clim. Past, 10, 221–250, doi:10.5194/cp-10-221-2014, 2014.
Schrag, D. P.: Effect of diagenesis on the isotopic record of late Paleogene tropical sea surface temperatures, Chem. Geol., 161, 215–224, 1999.
Schrag, D. P., DePaolo, D. J., and Richter, F. M.: Reconstructing past sea surface temperatures: correcting for diagenesis of bulk marine carbonate, Geochim. Cosmochim. Ac., 59, 2265–2278, 1995.

CPD
11, 243–278, 2015

Sexton, P. F., Wilson, P. A., and Pearson, P. N.: Microstructural and geochemical perspectives on planktic foraminiferal preservation: “Glassy” versus “Frosty”, Geochem. Geophy. Geosy., 7, Q12P19, doi:10.1029/2006GC001291, 2006.
Shackleton, N. J. and Kennett, J. P.: Paleotemperature history of the Cenozoic and the initiation of Antarctic glaciation: oxygen and carbon isotope analyses in DSDP sites 277, 279, and 281, Washington DC, US Government Printing Office, Initial reports of the Deep Sea Drilling Project, 29, 743–755, 1975.
Slotnick, B. S., Dickens, G. R., Nicolo, M., Hollis, C. J., Crampton, J. S., Zachos, J. C., and Sluijs, A.: Numerous large amplitude variations in carbon cycling and terrestrial weathering throughout the latest Paleocene and earliest Eocene, J. Geol., 120, 487–505, 2012.
Sluijs, A., Bowen, G., Brinkhuis, H., Lourens, L., and Thomas, E.: The Palaeocene-Eocene Thermal Maximum super greenhouse: biotic and geochemical signatures, age models and mechanisms of global change, in: Deep Time Perspectives on Climate Change: Marrying the Signal From Computer Models and Biological Proxies, edited by: Willliams, M. et al., The Geological Society of London, Special Publication, London, 323–347, 2007.
Sluijs, A., Bijl, P. K., Schouten, S., Röhl, U., Reichart, G.-J., and Brinkhuis, H.: Southern ocean warming, sea level and hydrological change during the Paleocene–Eocene thermal maximum, Clim. Past, 7, 47–61, doi:10.5194/cp-7-47-2011, 2011.
Stanley, S. M. and Hardie, L. A.: Secular oscillations in the carbonate mineralogy of reef-building and sediment-producing organisms driven by tectonically forced shifts in seawater chemistry, Palaeogeogr. Palaeocl., 144, 3–19, 1998.
Svensen, H.: Release of methane from a volcanic basin as a mechanism for initial Eocene global warming, Nature, 429, 542–545, 2004.
Taylor, K. W. R., Huber, M., Hollis, C. J., Hernandez-Sanchez, M. T., and Pancost, R. D.: Re-evaluating modern and Palaeogene GDGT distributions: implications for SST reconstructions, Global Planet. Change, 108, 158–174, 2013.
Tierney, J. E. and Tingley, M. P.: A Bayesian, spatially-varying calibration model for the TEX_{86} proxy, Geochim. Cosmochim. Ac., 127, 83–106, 2014.
Villasante-Marcos, V., Hollis, C. J., Dickens, G. R., and Nicolo, M. J.: Rock magnetic properties across the Paleocene–Eocene Thermal Maximum in Marlborough, New Zealand, Geol. Acta, 7, 229–242, 2009.
Wilkinson, B. H. and Algeo, T. J.: The sedimentary carbonate record of calcium magnesium cycling, Am. J. Sci., 289, 1158–1194, 1989.

CPD
11, 243–278, 2015

Zachos, J. C., Stott, L. D., and Lohmann, K. C.: Evolution of early Cenozoic marine temperatures, Paleoceanography, 9, 353–387, 1994.
Zachos, J. C., Pagani, M., Sloan, L. C., Thomas, E., and Billups, K.: Trends, rhythms, and aberrations in global climate 65 Ma to present, Science, 292, 686–693, 2001.
Zachos, J. C., Wara, M. W., Bohaty, S., Delaney, M. L., Petrizzo, M. R., Brill, A., Bralower, T. J., and Premoli-Silva, I.: A transient rise in tropical sea surface temperature during the Paleocene–Eocene thermal maximum, Science, 302, 1551–1554, 2003.
Zachos, J. C., Schouten, S., Bohaty, S., Quattlebaum, T., Sluijs, A., Brinkhuis, H., Gibbs, S. J., and Bralower, T. J.: Extreme warming of mid-latitude coastal ocean during the Paleocene–Eocene Thermal Maximum: inferences from TEX86 and isotope data, Geology, 34, 737–740, 2006.
Zachos, J. C., Dickens, G. R., and Zeebe, R. E.: An early Cenozoic perspective on greenhouse warming and carbon-cycle dynamics, Nature, 451, 279–283, 2008.
Zachos, J. C., McCarren, H., Murphy, B., Röhl, U., and Westerhold, T.: Tempo and scale of late Paleocene and early Eocene carbon isotope cycles: implications for the origin of hyperthermals, Earth Planet. Sc. Lett., 299, 242–249, 2010.

CPD
11, 243–278, 2015

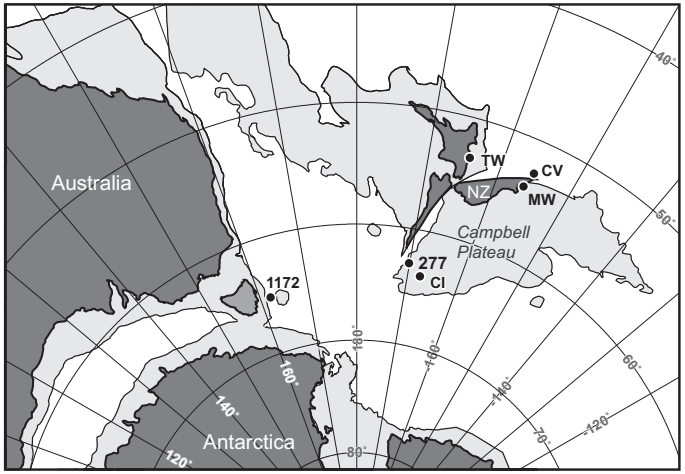

Figure 1. Location of DSDP Site 277 on a tectonic reconstruction for the southwest Pacific during the early Eocene (~ 54 Ma) (Cande and Stock, 2004). Other localities mentioned in the text are also shown: ODP Site 1172, Campbell Island (CI), Tawanui (TW), Mid-Waipara River (MW) and Clarence Valley (CV).

CPD
11, 243–278, 2015

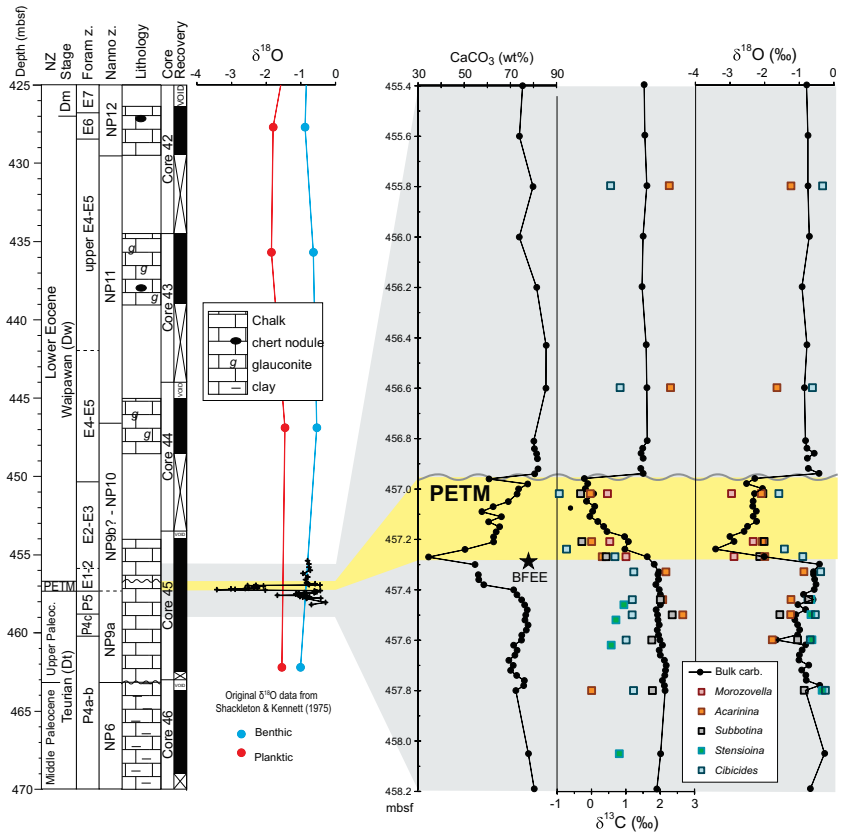

Figure 2. Biostratigraphy, lithologies, carbonate content and stable isotopes from bulk carbonate and foraminifera across the Paleocene–Eocene transition at DSDP Site 277. Abbreviations: Mangaorapan local stage (Dm); Paleocene–Eocene Thermal Maximum (PETM), Benthic Foraminiferal Extinction Event (BFEE).

CPD
11, 243–278, 2015

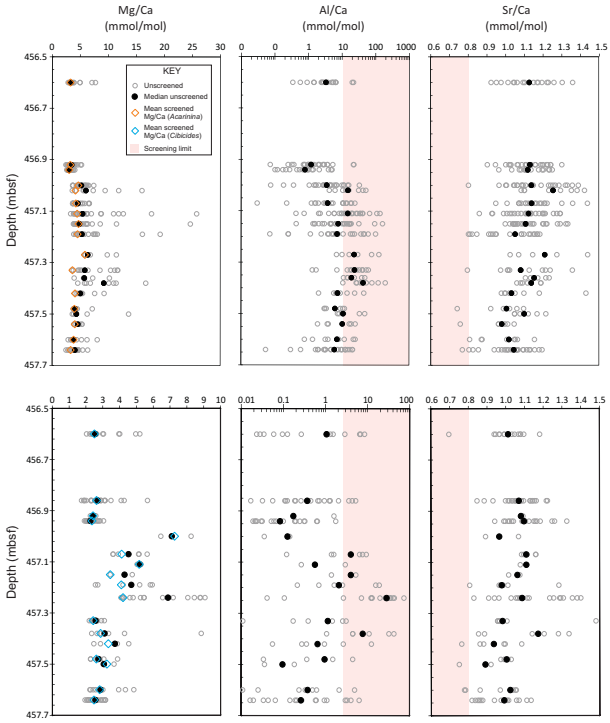

Figure 3. Trace element–depth plot for *Acarinina* and *Cibicides* across the PETM interval, showing all the measured Mg/Ca, Al/Ca and Sr/Ca values measured, and the corresponding decrease of the mean Mg/Ca value when Al/Ca and Sr/Ca screening protocols are imposed on the raw dataset. The pink shaded areas show the data points removed by the application of the screening limits, with the consequent decrease in Mg/Ca ratio (and therefore temperature) shown by the black circles (median of unscreened Mg/Ca) and the orange and blue diamonds (mean screened Mg/Ca ratios for *Acarinina* and *Cibicides* respectively). Note the change in scale on the horizontal axes for Mg/Ca and Al/Ca between the *Acarinina* and *Cibicides* records.

CPD
11, 243–278, 2015

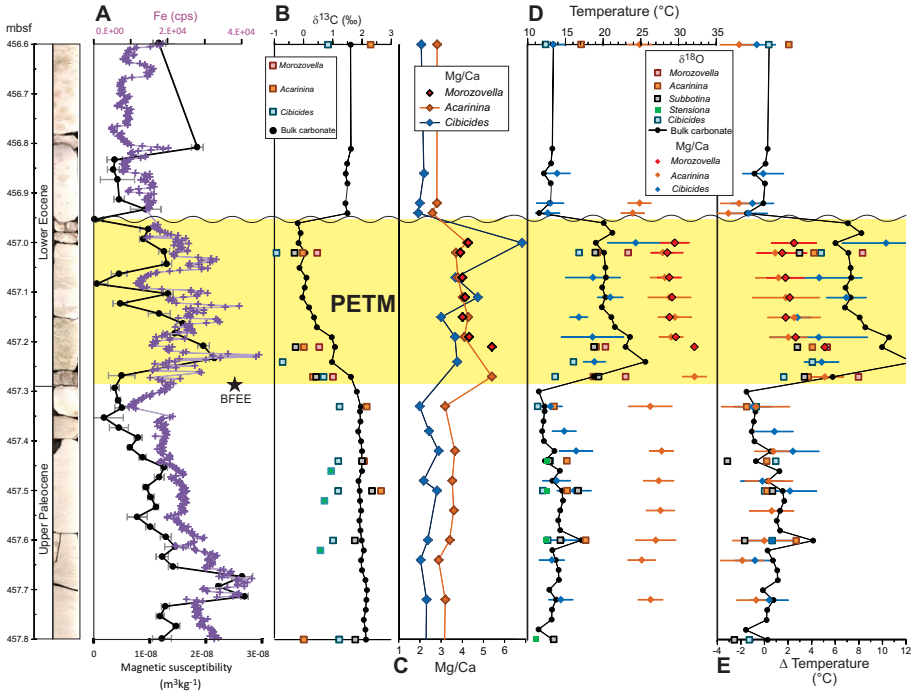

Figure 4. Variation in **(a)** Fe content and magnetic susceptibility; **(b)** $\delta^{13}C$; **(c)** Mg/Ca ratios; **(d)** paleotemperatures derived from $\delta^{18}O$ values and Mg/Ca ratios; and **(e)** changes in paleotemperature relative to average Paleocene values.

CPD
11, 243–278, 2015

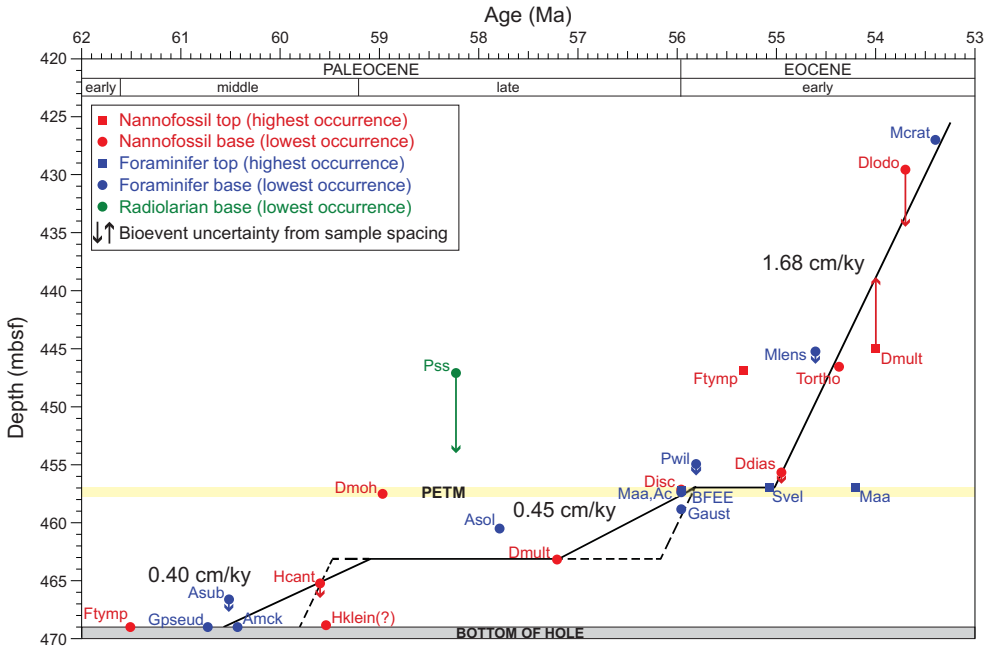

Figure 5. Age–depth plot for the Paleocene–Eocene transition at DSDP Site 277. Abbreviations for species names are explained in Table S7.

CPD
11, 243–278, 2015

PETM at DSDP Site 277

C. J. Hollis et al.

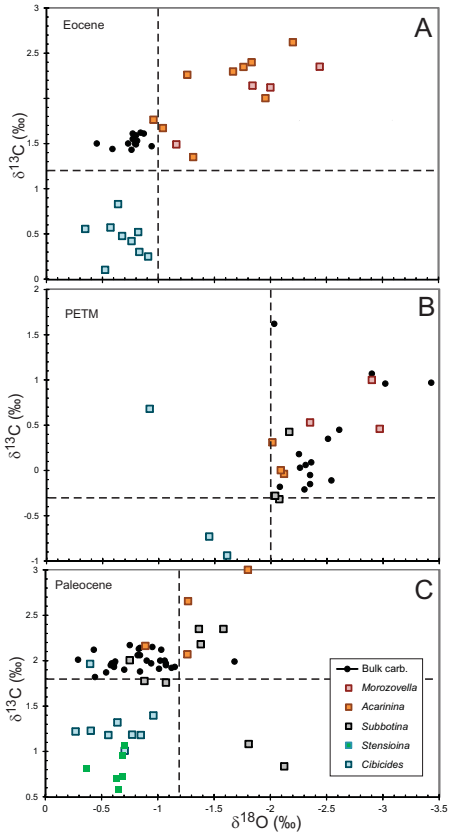

Figure 6. Cross plot of stable isotope ($\delta^{13}C$, $\delta^{18}O$) values for bulk carbonate, *Cibicides*, *Acarinina* and *Morozovella* within the Paleocene, Paleocene–Eocene Thermal Maximum (PETM), and overlying Eocene.

CPD
11, 243–278, 2015

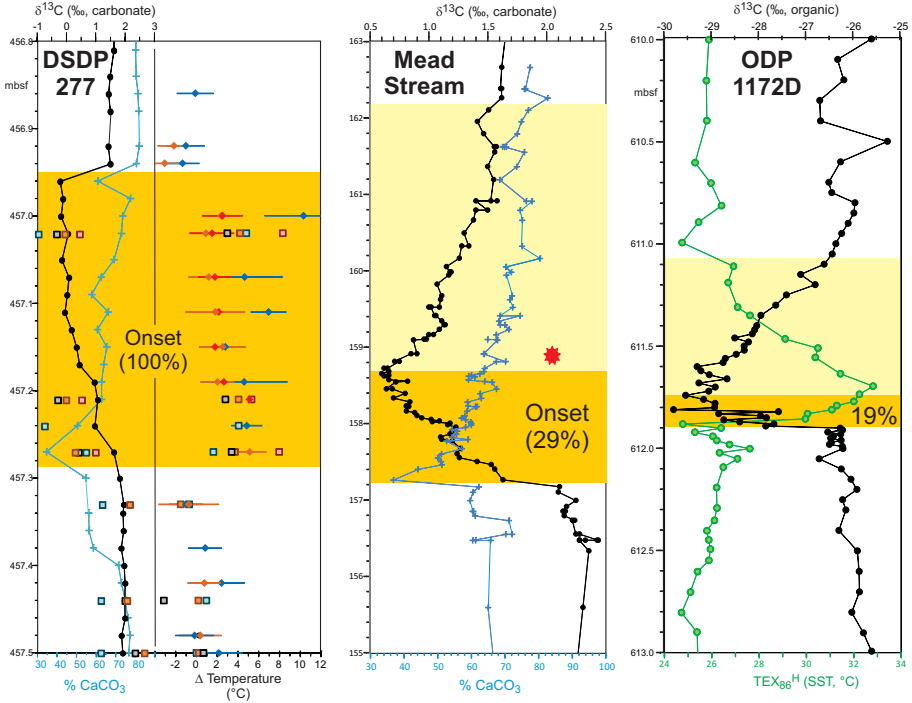

Figure 7. Comparison of records of the Paleocene–Eocene thermal maximum (PETM) at DSDP Site 277, ODP Site 1172 and Mead Stream. Symbols for DSDP Site 277 as in Fig. 4. Note the bulk carbonate $\delta^{18}O$ record is not plotted as a guide for relative temperature change at DSDP 277 because the record is inferred to be affected by diagenesis. The Red star marks single incursion of low-latitude radiolarians at Mead Stream (Hollis, 2006).

CPD
11, 243–278, 2015